

# HiSST: 4th International Conference on High-Speed Vehicle Science Technology

22 -26 September 2025, Tours, France



# Dynamic stability testing in DLR Wind Tunnels using a new free oscillation device

J. Zhai, T. Gawehn, A. Gülhan 1

#### **Abstract**

A new dynamic stability test device has been designed and manufactured for the wind tunnels of DLR, based on the free-oscillation measurement technique. A key feature of the device is its versatility: it can be used in different wind tunnels, covering flow regimes from subsonic to hypersonic. By exchanging the cross-springs, free oscillation tests can be performed in pitch, yaw, or roll. A series of cross-springs with different stiffness values are available, enabling tests with models of varying load and stiffness requirements. The device is suitable for both capsule-like and lifting body configurations.

The first application was a dynamic pitch stability test with the ReFEx model (Reusable Flight Experiment of DLR), a lifting space vehicle. The results demonstrated dynamic stability along the designed trajectory. For this test, data were evaluated both from the cross-spring signal and from Schlieren images. Both methods showed excellent agreement, confirming the validity of the signal processing approach.

A second application was a dynamic pitch stability test with an Inflatable Heat Shield model in the framework of EFESTO-2, a Horizon Europe project. Two cross-springs with different stiffness values were used, yielding test data at different reduced pulsations. Additional Reynolds number variations were performed, allowing the influence of reduced pulsation and Reynolds number on the dynamic derivatives to be assessed.

**Keywords**: Wind tunnel testing, Free oscillation, Reentry capsule, Space vehicle

## **Nomenclature**

Latin		Р	Axial force acting on a cross-spring
b	Width of the leaf-spring	р	Pressure
$C_{m\alpha}$	Aerodynamic stiffness	q	Dynamic pressure
$C_{mq}$ +	$C_{m\dot{\alpha}}$ Aerodynamic damping	R	Bridge signal
C <sub>y</sub>	Stiffness of the cross-spring	t	Time
C <sub>y0</sub>	Stiffness at zero axial force	u	Velocity
Cyf	Stiffening factor		
ď	Thickness of the leaf-spring	Greek	
Е	Young's modulus	α	Half angle between the two leaf-
F	Normal force acting on a cross-spring		springs
$F_x$	Axial force	θ	Deflection angle
M	Moment	ζ	Reduced pulsation
I	Second area moment	δ	Decrement
Iy	Moment of inertia	σ	Stress
k	Strain gauge factor	ω	Angular frequency
L	Length of the leaf-spring		

<sup>&</sup>lt;sup>1</sup> German Aerospace Center (DLR), Institute of Aerodynamics and Flow Technology, Supersonic and Hypersonic Technologies Department, Linder Höhe, 51147 Köln, Germany, Junnai.Zhai@dlr.de

HiSST-2025-0092 Page | 1 Dynamic stability testing in DLR Wind Tunnels using a new free oscillation device Copyright © 2025 by author(s)

-

0 Stagnation

Subscripts Ref Reference

### 1. Introduction

Dynamic stability is a critical issue during atmospheric entry and re-entry of both capsule-type and lifting-body vehicles, as it is essential for mission success. To address this, wind tunnel testing techniques for predicting dynamic stability have been developed at DLR [1]. One such method is the sting-supported free oscillation technique, where the model is mounted on a cross-spring and allowed to oscillate freely in one plane within the wind tunnel flow. Compared to forced oscillation methods, this technique directly captures the natural response of the system, including damping effects and nonlinear behavior.

One early application at DLR was performed in the 2010s with an EXOMARS capsule model in the trisonic wind tunnel TMK. A cross-spring instrumented with strain gauges measured the dynamic motion of the model, while a pneumatic mechanism provided deflection and release. Tests were conducted at Mach numbers between 1.8 and 3.5, with variations in Reynolds number and angle of attack. Later, another device was developed to test the IXV model in TMK, later also equipped with fins and flaps [2] [3] [4] [5]. These tests covered a Mach number range from 0.5 to 2.0, and aerodynamic derivatives were successfully determined for the required configurations.

Building on this experience, a new versatile test device has been developed. It can be used for both capsule-type and lifting-body vehicles. By exchanging the cross-spring, free oscillation tests can be performed in pitch, roll, and yaw. For each degree of freedom, springs with different stiffness are available, allowing the device to accommodate models with varying load and stiffness requirements.

This paper first provides an overview of the new test device, followed by results from tests with both a capsule and a lifting-body model.

# 2. The new dynamic test device

The new test device was developed for conducting free oscillation measurements and is composed of two key components: a cross-spring and a release mechanism. The cross-spring constrains the model to oscillations in one single degree of freedom while suppressing undesired motions in other degrees of freedom. This ensures that the measured dynamics can be directly attributed to the targeted oscillatory motion, improving the accuracy and reliability of the results. The release mechanism complements this function by holding the model securely in a predefined deflected position and then releasing it in a controlled and repeatable manner. This precise triggering of free oscillations under wind tunnel conditions enables consistent data acquisition and facilitates the comparison of different test configurations.

Fig. 1 illustrates the design of the new test device. The setup is compact, integrating all key components within a limited space. The model is attached to the cross-spring through a dedicated adapter. The cross-spring is mounted on a short sting, which is inserted into the main sting to provide stable support. The release mechanism is integrated into both the short and main sting, thereby minimizing external interference with the flow field.

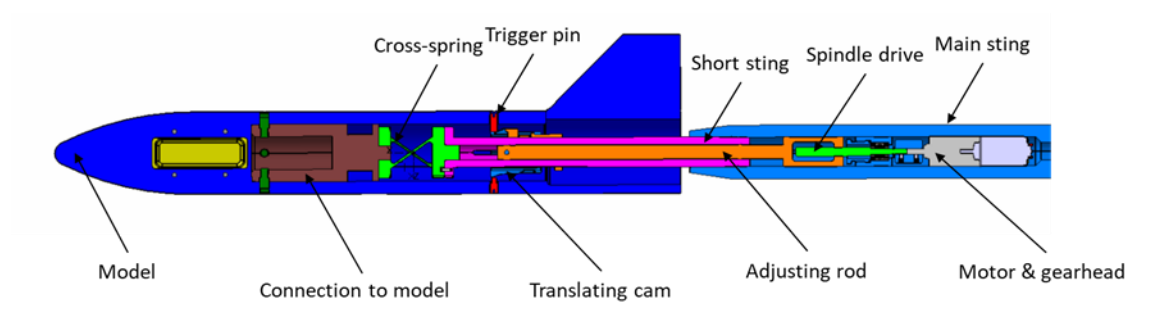


Fig. 1. Assembly of the dynamic test device with the model

The connection to the model is identical to that used for static tests with an internal balance, allowing the same model to be employed for both static and dynamic investigations. This not only reduces model costs but also provides an important advantage: since the trim angle and aerodynamic stiffness coefficients can be obtained from both test types, a direct comparison of these parameters is possible, thereby increasing confidence in the results. Furthermore, the use of an adapter between the cross-spring and the model enables standardization of the dynamic test device. With this design, a single device can be applied to various models, requiring only the selection of a suitable cross-spring to match the specific test configuration.

# 2.1. Release mechanism

As shown in Fig. 1, the release of the model is achieved by two translating cams positioned on opposite sides of the model (top and bottom in the case of the pitching test). The follower, or trigger pin, is fixed to the model, while the cams are driven by a stepper motor via a spindle drive, ensuring precise and repeatable operation.

The test process, illustrated in Fig. 2, consists of a sequence of controlled phases. Initially, the model is held in its neutral (non-deflected) position by two trigger pins. By activating the stepper motor, the spindle drive moves the cams, which deflect the model from its neutral position. At maximum deflection, the upper pin slides onto a sleeve, holding the model in place, while further cam motion disengages the lower pin. Release occurs when the upper pin slides off the cam edge, allowing the model to oscillate freely about its equilibrium position. At this stage, the dynamic measurement begins [6].

To recapture the model, the motor reverses the cam motion. The upper pin re-engages the cam, pushing the sliding sleeve aside so that the pin can follow the cam contour. As the cam rises, the model is again deflected until, at maximum deflection, the sliding sleeve resets under spring force and the system becomes ready for the next triggering. With continued cam motion, the pins follow the cam contours, gradually reducing the deflection until the model is returned to its neutral position and fixed, completing the cycle.

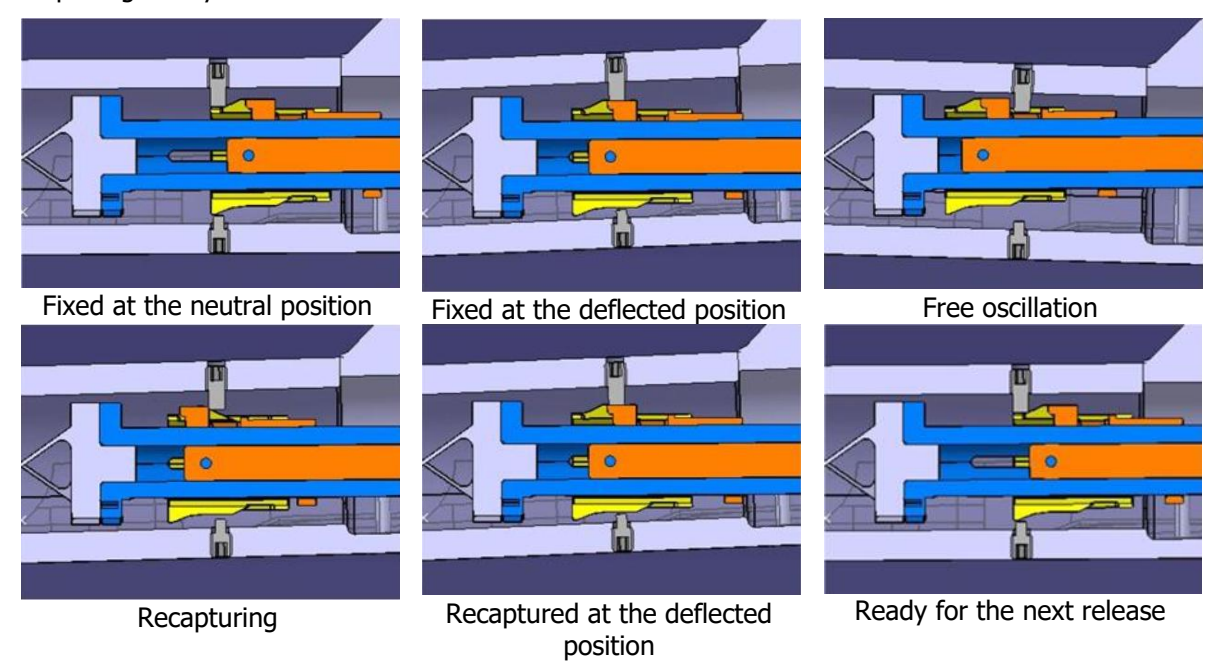


Fig. 2. Major phases of the test process

#### 2.2. Cross-spring

The key component of the dynamic test device is the elastic cross-spring. It is formed by symmetrically crossing two leaf springs along their length, enabling rotational motion through elastic bending deflection. This configuration provides high rotational compliance in the oscillation plane while maintaining substantial stiffness in the transverse directions.

The mechanical behavior of the cross-spring can be described using bending beam theory, which provides accurate approximations for its characteristics. The rotational stiffness is expressed as:

$$c_y = \frac{M}{\theta} = \frac{2EI}{L} - \frac{LP}{6\cos\alpha} = c_{y0} + c_{yf}P$$
 (1)

Eq. (1) shows that the axial force influences the stiffness of the cross-spring. The effect is essentially linear: a negative axial force leads to an increase in stiffness, the so-called stiffening effect. This influence must be calibrated and accounted for in the data reduction process to ensure correct results.

The maximum bending stresses in leaf-springs occur in the middle and are obtained as:

$$\sigma_{1,max} = \left(\frac{dE}{2L} + \frac{FL}{8bd^2 \sin \alpha} - \frac{PL}{8bd^2 \cos \alpha}\right)\theta \tag{2}$$

$$\sigma_{2,max} = \left(\frac{dE}{2L} - \frac{FL}{8hd^2\sin\alpha} - \frac{PL}{8hd^2\cos\alpha}\right)\theta\tag{3}$$

When strain gauges are applied at the mid-span of one leaf-spring and connected in a full-bridge configuration, the resulting signal is proportional to the deflection angle of the cross-spring. The relation between the bridge output and the deflection angle is obtained as:

$$R = k\left(\frac{d}{2L} + \frac{FL}{8bd^2E\sin\alpha} - \frac{PL}{8bd^2E\cos\alpha}\right)\theta\tag{4}$$

It can be observed that both the axial force and the normal force influence the sensitivity of the cross-spring, i.e., the ratio of signal to deflection angle. In the free oscillation tests, however, the deflections are generally small (below 3°), so the sensitivity can be considered constant within a given test run. This assumption was verified during the ReFEx test campaign by comparing the deflection derived from the cross-spring signal with that obtained from Schlieren images. Consequently, for the evaluation of the test data, the cross-spring signal is used directly instead of the deflection angle.

The cross-spring can be designed using Eq. (1) - (4). Its layout is shown in Fig. 3. To increase lateral stiffness, one of the two leaf-springs is divided into two equal parts and arranged symmetrically. The analytical results presented above remain valid for this configuration.

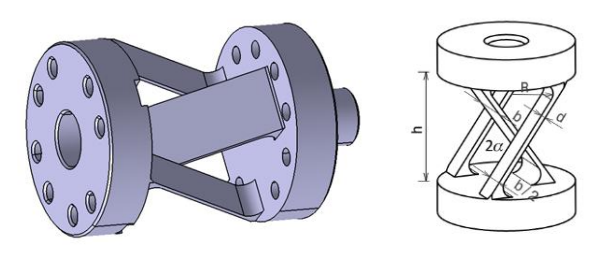


Fig. 3. Layout of the cross-spring

Three cross-springs were designed using the above equations, with nominal rotational stiffness values of 1 Nm/rad (CS1), 4 Nm/rad (CS4), and 10 Nm/rad (CS10), respectively. All three share the same overall dimensions, with a diameter of 17 mm and a height of 22 mm, and differ only in the thickness of the leaf-springs, which are 0.39 mm, 0.62 mm, and 0.84 mm.

To validate the design, the three cross-springs were analyzed using the FEM tool Ansys R16.1. The simulations examined stiffness, sensitivity, stress, and buckling load, with the results summarized in Table 1. The differences between the analytical predictions and the FEM results were below 8%, confirming the validity of the analytical method.

**Table 1.** Comparison of the designed and FEM-calculated properties of the cross-springs

	Symbol	CS1		CS4			CS10				
Parameter		design	FEM	difference	design	FEM	difference	design	FEM	difference	Unit
Stiffness	c <sub>y0</sub>	1.01	0.97	3.7%	4.05	3.82	5.6%	10.06	9.34	7.2%	Nm/rad
Sensitivity	kθ	1808.27	1895.31	-4.8%	1137.46	1216.87	-7.0%	839.56	823.00	2.0%	deg/V/V
Stress at deflection 2.5°	σθ	144.44	146.92	-1.7%	229.63	236.39	-2.9%	311.14	314.68	-1.1%	N/mm²
Buckling load	P <sub>cr</sub>	-1961.7	-2118.3	-8.0%	-7881.6	-8142.9	-3.3%	-19601.0	-21044	-7.4%	N

The cross-springs were manufactured from heat-treated high-grade steel 1.6580.05 (DIN/EN 30CrNiMo8 +QT). In the first step, the raw parts underwent stress-relief annealing at 510 °C. All surfaces, except for the leaf-springs, were then machined to their final dimensions by turning and milling. The leaf-springs were subsequently produced with high precision using wire and sinker EDM, ensuring the required dimensional accuracy and surface quality for reliable operation in the dynamic test device.

Four linear strain gauges were applied to the two outer leaf-springs and connected in a full Wheatstone bridge. This configuration provides high sensitivity and compensates for temperature effects, enabling accurate measurement of the cross-spring deflection. Fig. 4 shows the cross-spring instrumented with strain gauges.



Fig. 4. Instrumented cross-spring

The final parameters for the evaluation of the wind tunnel tests are obtained through calibration, which requires both static and dynamic procedures. The purpose of the static calibration is to determine the cross-spring stiffness and the strain-gauge sensitivity for measuring the deflection angle. As indicated in Eq. (1), the stiffness is a linear function of the axial force, and this effect must therefore be considered during calibration. The static calibration device is shown on the left in Fig. 5. Axial forces are generated by applying calibration weights symmetrically on a shaft, while the deflection moment is introduced by placing defined weights at pre-determined positions along a horizontal bar. The corresponding deflection angle is measured optically by tracking the displacement of a reflected laser beam.

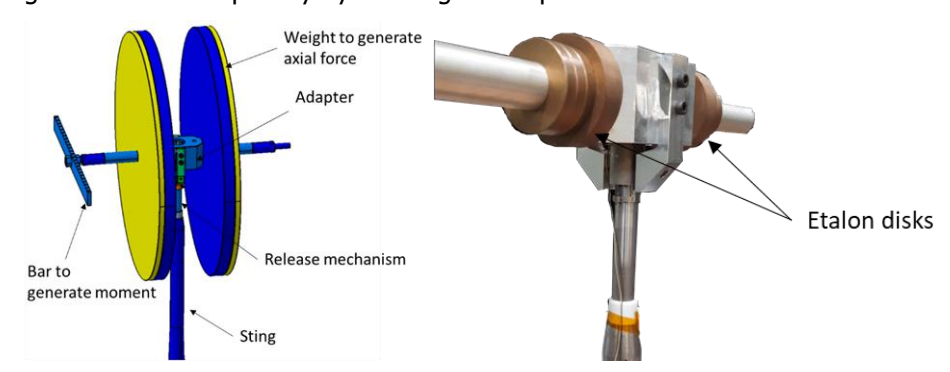


Fig. 5. Calibration device. Left: static calibration; right: dynamic calibration

The results of the stiffness calibration of the 4 Nm/rad cross-spring are presented on the left in Fig. 6. The dependency of the stiffness on the axial force is clearly evident. The estimated stiffness can be expressed as:

$$c_y = 3.3642 + 0.00265F_x \tag{5}$$

The residual load errors - defined as the difference between the estimated cross-spring moment and the applied moment - are plotted as a function of the calibration point on the right in Fig. 6. The distribution demonstrates that the mathematical model used for the estimation is appropriate.

HiSST-2025-0092 Page | 5 Copyright © 2025 by author(s)

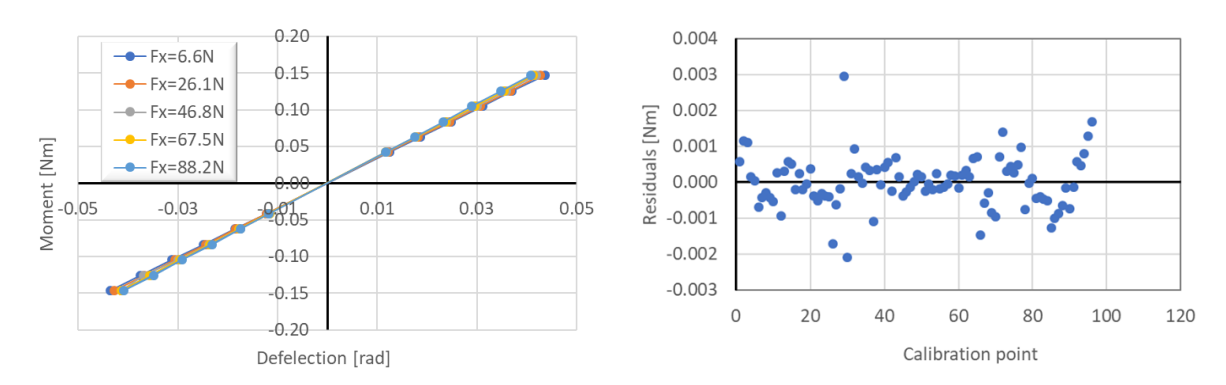


Fig. 6. Stiffness calibration of the 4 Nm/rad cross-spring: calibration curve and residuals

Fig. 7 presents the results of the sensitivity calibration of the 4 Nm/rad cross-spring. The estimated deflection can be calculated as:

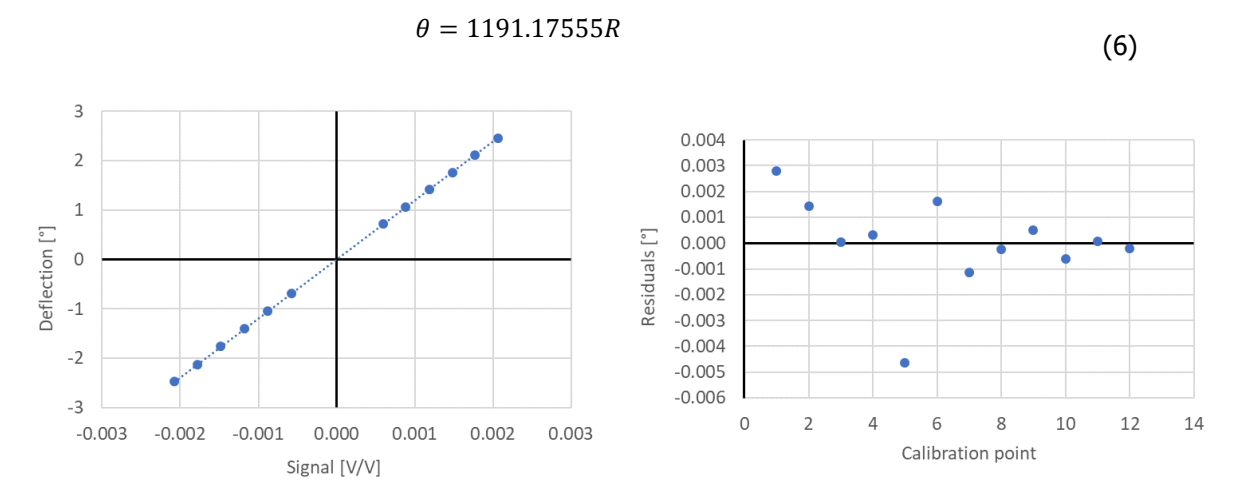


Fig. 7. Sensitivity calibration of the 4 Nm/rad cross-spring: calibration curve and residuals

The main objective of the dynamic calibration is to determine the damping characteristics of the cross-spring in the absence of flow, referred to as tare damping. For this purpose, a dedicated dynamic calibration device, shown on the right in Fig. 5, was employed. It is equipped with catches for etalon disks of known geometry and inertia properties. The device is attached to the cross-spring, and the assembly is mounted on the sting containing the release mechanism, which is used to initiate the free oscillations.

The damping of the cross-spring depends on the oscillation frequency. Therefore, the disk combinations were selected to provide reference frequencies covering the entire design range. Previous experiments have shown that the damping decrement is independent of axial force and depends solely on the angular frequency. Furthermore, atmospheric conditions were found to have no significant influence on the damping measurements.

Fig. 8 presents the damping decrement as a function of angular frequency for the 4 Nm/rad cross-spring. Linear regression was applied, with the residuals (Fig. 8, right) demonstrating an acceptably small error margin. For verification, the damping decrement obtained from a dry run during the wind tunnel test (red point in Fig. 8) was added and found to align well with the regression curve.

The relation can be expressed as:

$$\delta_c = 0.001863\omega - 0.033332\tag{7}$$

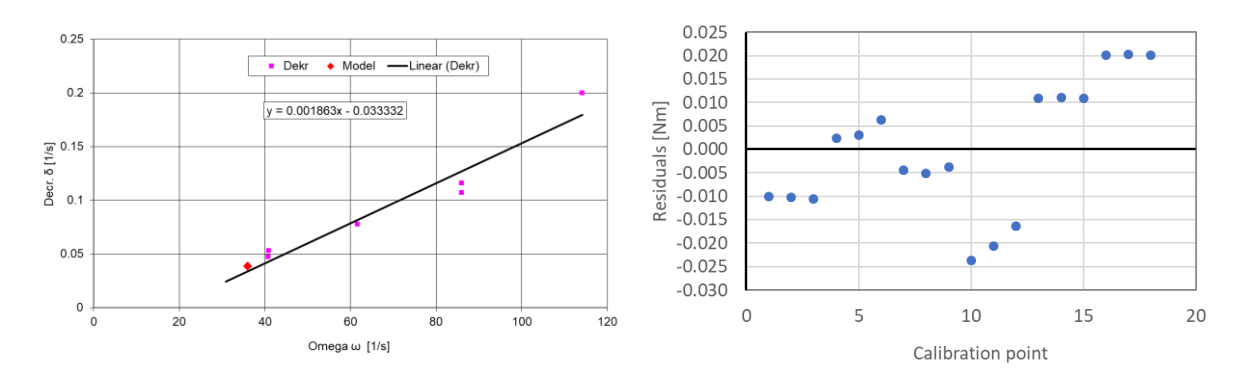


Fig. 8. Damping characteristic of the 4 Nm/rad cross-spring

# 2.3. Options for yaw and roll stability testing

For the dynamic test of yaw stability, the model is mounted at a rolling angle of 90°. To accommodate this configuration, provision of two trigger-pin holes in the horizontal plane of the model is required, while the remaining setup can be applied without modification.

For the roll stability tests, a cross-spring of the type shown in Fig. 9 can be employed. It follows the same principle as the cross-spring in Fig. 3, but with a modified connection that allows rotation about the longitudinal axis.



Fig. 9. Cross-spring for the roll stability testing, adapted from a product of C-Flex Bearing Co., Inc.

Fig. 10 shows the test setup for the roll dynamic stability testing. Compared to the pitch stability setup in Fig. 1, only a few modifications are required:

- the translating cam controlling the release process,
- · the cross-spring and its connections, and
- the model connection

These limited changes enable the same overall test device to be adapted efficiently for roll stability investigations.

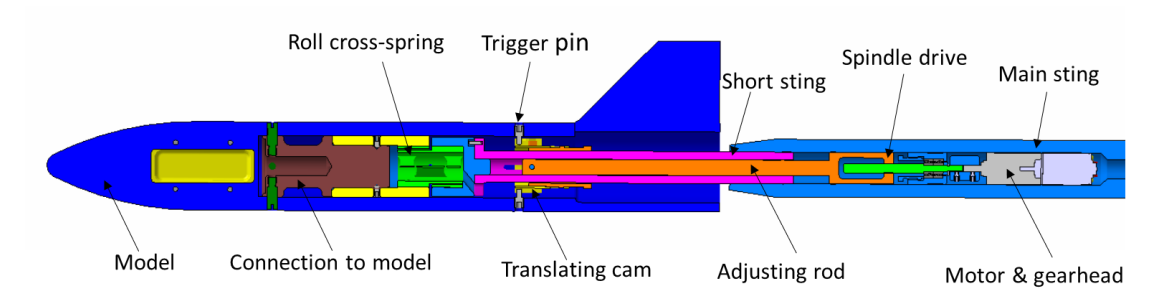


Fig. 10. Test setup for the dynamic roll stability

The device was also adapted for the GHGV test campaign. In this project, the rotational axis was located close to the model surface, requiring specially designed cross-springs. This application further demonstrates the versatility of the device [7].

# 3. Dynamic stability test with ReFEx

ReFEx (Reusability Flight Experiment) is a DLR project aimed at demonstrating key technologies for aerodynamically controlled returning stages. It involves flying a generic winged booster stage on a sounding rocket and actively guiding its trajectory through hypersonic, supersonic, and transonic regimes down to Mach 0.8, which marks the end of the scientific phase of the flight. Beyond this point, the remaining descent to touch-down is routine in civil aviation and therefore not part of the scientific objectives for demonstrating fully aerodynamic RLV return. The vehicle itself is a generic winged booster stage equipped with movable canards, a vertical stabilizer with rudder, and fixed delta wings, as shown in Fig. 11 [8].

In the course of the project, several wind tunnel tests were performed to validate the CFD results and support the aerodynamic databases [9]. The following section summarizes the dynamic stability test conducted with the newly developed device.

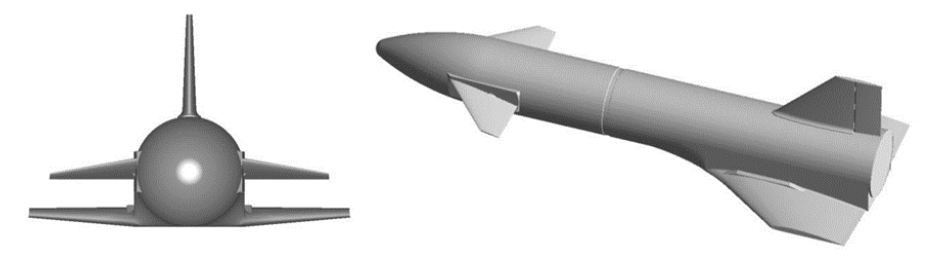


**Fig. 11.** ReFEx geometry

# 3.1. Experimental Apparatus

The dynamic stability test with the ReFEx model was carried out in the Trisonic Wind Tunnel (TMK). TMK features a closed rectangular test section measuring  $0.6 \,\mathrm{m} \times 0.6 \,\mathrm{m}$  and operates across subsonic, transonic, and supersonic regimes, covering Mach numbers from  $0.5 \,\mathrm{to} \,5.7$ . As sketched in Fig. 12, pressurized air from a 55 bar reservoir passes through a storage heater and settling chamber before being accelerated in an adaptable Laval nozzle. In the test section, nearly constant flow conditions are achieved, after which the flow is decelerated in a downstream diffuser system. Depending on Mach and Reynolds number conditions, maximum run times of up to 60 seconds are possible [10].

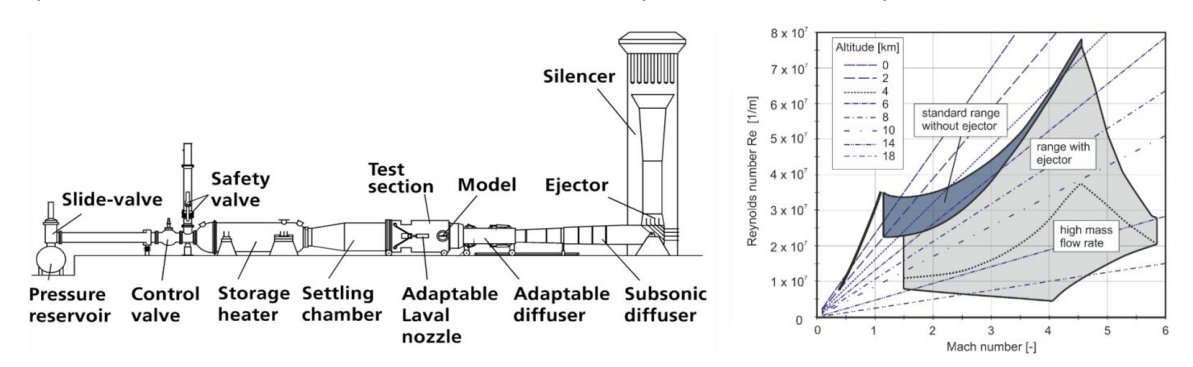


Fig. 12. Schematic drawing (left) and performance map (right) of TMK

Since the requirements for the static model, such as blockage and structural loads, also applied to the dynamic configuration, the existing static model was adapted for use in the dynamic test. The modifications focused on adjusting the model's center of gravity (CoG) and providing an interface for mounting on the dynamic test device.

The first requirement was addressed by designing a new vertical tail using a suitable material, while the second was fulfilled by positioning the model appropriately on the dynamic test device. The left image in Fig. 13 shows the final configuration of the dynamic model. The coordinate system is defined with its origin at the vehicle's CoG, located at 57% of the total model length from the nose. Components highlighted in cyan were retained from the static model, whereas the magenta part was newly manufactured for the dynamic test.

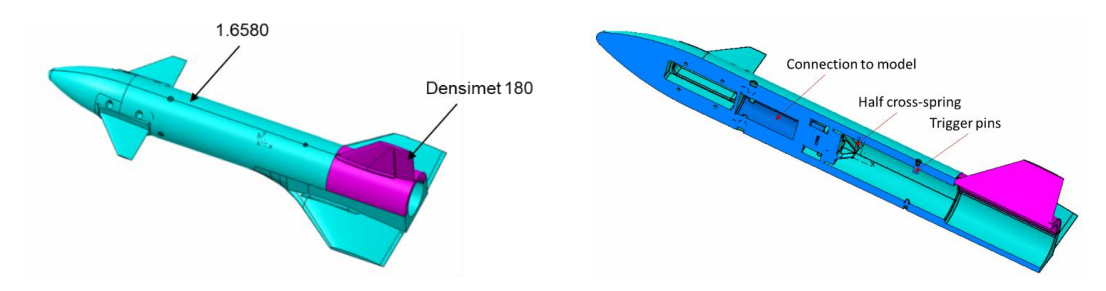


Fig. 13. Design of the dynamic model. Left: materials; Right: sectional view of the model

#### 3.2. Test conditions

For the dynamic stability test, an additional similarity parameter to be considered - besides Mach and Reynolds number - is the reduced pulsation (RFP). This nondimensional parameter is defined as:

$$\zeta = \frac{\omega L_{ref}}{u_{\infty}} \tag{8}$$

The angular frequency for wind tunnel tests with a cross-spring can be calculated as:

$$\omega = \sqrt{\frac{-M_{\theta} + c_{y}}{I_{y}}} \tag{9}$$

The aerodynamic stiffness can be estimated from the static stability test.

In wind tunnel tests, the objective is to reproduce the three similarity parameters of free flight as closely as possible. Mach and Reynolds number similarities were already addressed in the static test, which defined the required wind tunnel flow conditions such as Mach number, total pressure, and temperature. Since the same model was used for both static and dynamic testing, these flow parameters could be directly applied to the dynamic test in TMK.

Reduced pulsation similarity can be achieved either by adapting the model's moment of inertia or by selecting an appropriate cross-spring. In this study, the latter approach was adopted. Fig. 14 compares the reduced pulsation in free flight with the wind tunnel values obtained using the three available crosssprings. The value obtained with CS1 is closest to flight conditions; however, the difference compared to CS4 is minimal. Since CS4 provides greater stability, it was selected for the dynamic stability tests.

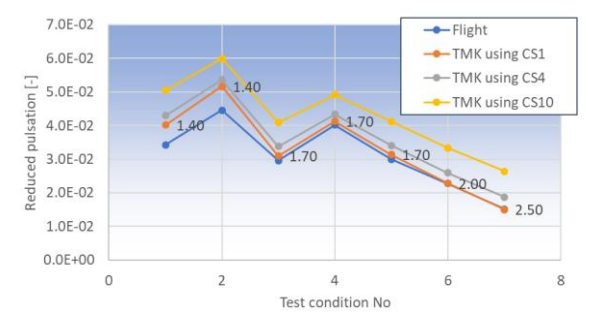


Fig. 14. Comparison of the flight and wind tunnel reduced pulsation. Label: Mach number The final test conditions are listed in Table 2.

**Table 2.** Flow conditions for the dynamic test with ReFEx in TMK

Case No		TMF	Model				
	Mach	P <sub>0</sub> [bar]	$T_0[K]$	Re [milo.]	q∞ [bar]	Canard [°]	Roll [°]
1	1.4	2.08	288.15	6.78	0.90	5	0
2	1.4	2.08	288.15	6.78	0.90	10	0
3	1.7	2.32	288.15	7.02	0.95	0	0
4	1.7	2.32	288.15	7.02	0.95	5	0
5	1.7	2.32	288.15	7.02	0.95	10	0

HiSST-2025-0092 Page | 9 Copyright © 2025 by author(s)

6	2	2.78	288.15	7.51	0.99	0	0
7	2.5	3.81	288.15	8.12	0.98	0	0

#### 3.3. Test results

Before testing, the sting angle was adjusted using trim data from static tests and corrected for sting deformation. The wind tunnel was then brought to the desired flow condition with the release mechanism locked. The model was deflected to a preset angle, released, and its free oscillations recorded. Each configuration was tested three times with the CS4 cross-spring to ensure repeatability. If the neutral angle of attack (AoA) deviated by more than 0.1°, the sting setting was corrected and the test repeated. An example of the measured oscillation is shown in Fig. 15.

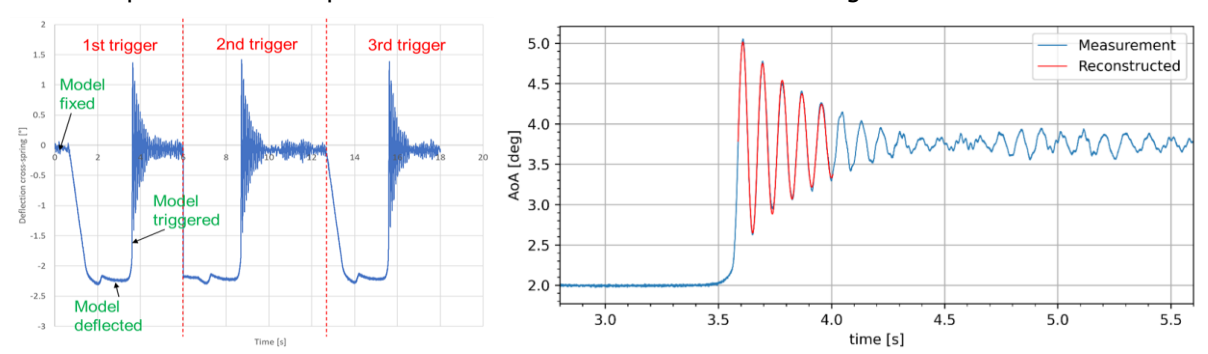


Fig. 15. Procedure of a test run (left) and approximated oscillation (right)

For the free oscillation test, the governing equation of motion can be expressed as:

$$I_{\nu} \ddot{\theta} + (k_{\nu} - M_{\dot{\theta}}) \dot{\theta} + (c_{\nu} - M_{\theta}) \theta = 0$$
 (10)

which can be transformed into the general form of a damped harmonic oscillator as:

$$\ddot{\theta} + 2 \delta \dot{\theta} + \omega_0^2 \theta = 0 \tag{11}$$

having the solution in the form:

$$\theta = \hat{\theta} e^{-\delta t} \cos(\omega t + \varphi) \tag{12}$$

The parameters in Eq. (12) were determined by fitting the measured deflection angle. An example of the approximated oscillation for one run is shown on the right in Fig. 15.

From these parameters, the aerodynamic stiffness coefficient and damping coefficient can be derived:

Aerodynamic stiffness: 
$$c_{m\alpha} = \frac{c_y - l_y(\omega^2 + \delta^2)}{q_{\infty} A_{Ref} L_{Ref}}$$
 (13)

Aerodynamic damping: 
$$\left(c_{mq} + c_{m\dot{\alpha}}\right) = \frac{(k_y - 2l_y\delta)u_\infty}{q_\infty A_{Ref}L_{Ref}^2}$$
 (14)

The aerodynamic stiffness coefficients are shown on the left in Fig. 16 as a function of Mach number, together with the corresponding static test results. A strong correlation is observed between the two methods despite their different measurement techniques, validating the accuracy and consistency of the dynamic test methodology applied in this study.

The aerodynamic damping derivatives are illustrated on the right inFig. 16. The results indicate strong damping in the supersonic regime. Moreover, the absolute values of the damping coefficients increase with decreasing Mach number, a trend consistent across all canard deflections (0°, 5°, and 10°).

Fig. 16. Aerodynamic damping coefficients (left) and aerodynamic stiffness coefficients (right), with canard deflection angle and trim AoA indicated

Schlieren pictures were recorded for all test runs. From the schlieren images, the AoA can be determined. This provides an additional method for calculating the dynamic derivatives. Since the AoA obtained from the Schlieren images is independent of the AoA measured by the cross-spring, the results serve as a verification of the cross-spring-based evaluation.

Fig. 17 presents the differences in aerodynamic stiffness and damping coefficients obtained from crossspring and Schlieren imaging. For the damping coefficients, the differences remain within ±0.1, except for Run 12 (0.27), which is still well below the uncertainty range of 0.2-0.5. The stiffness coefficient differences are minimal, within ±0.0003 1/°. These results confirm that both evaluation methods are consistent and equally applicable for determining dynamic derivatives.

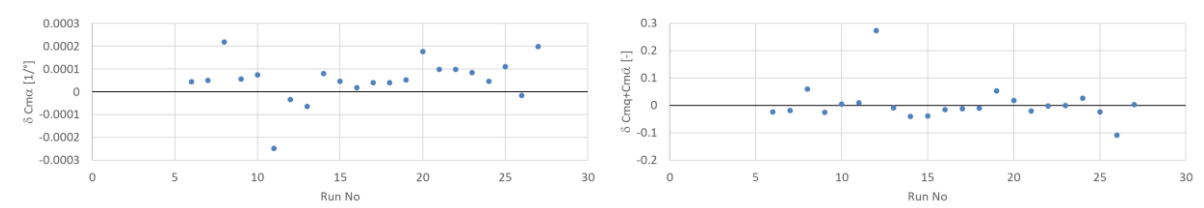


Fig. 17. Difference in aerodynamic damping coefficients (left) and in stiffness coefficients measured using cross-spring and Schlieren imaging

# 4. Dynamic stability test with EFESTO-2

EFESTO-2 is a European project funded under the Horizon Europe program and coordinated by Deimos Space (ES). The consortium includes ONERA (FR), DLR (DE), CIRA (IT), POLITO (IT), Deimos Engenharia (PT), and Pangaia-Grado Zero (IT). The project investigates key technologies for Inflatable Heat Shields (IHS), a breakthrough concept that can significantly increase payload capability and enhance recovery potential for future re-entry space missions [11].

One focus of EFESTO-2 is the investigation of aeroshapes with respect to aerodynamics and aerothermodynamics. For this purpose, both non-deformed and deformed IHS models were designed and tested in the DLR H2K and TMK wind tunnels to assess static and dynamic stability. A numerical fluid-structure interaction (FSI) study indicated that deformation in the supersonic regime is negligible [12]. Since the IHS is expected to experience dynamic stability issues in the lower supersonic regime, a dynamic test with the non-deformed aeroshape model was conducted in TMK using the abovementioned test device (Fig. 18) [13].

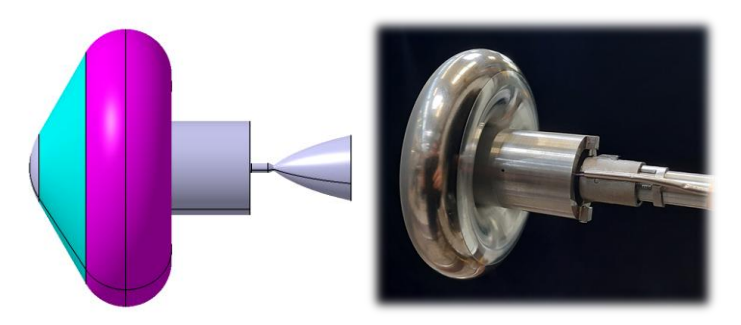
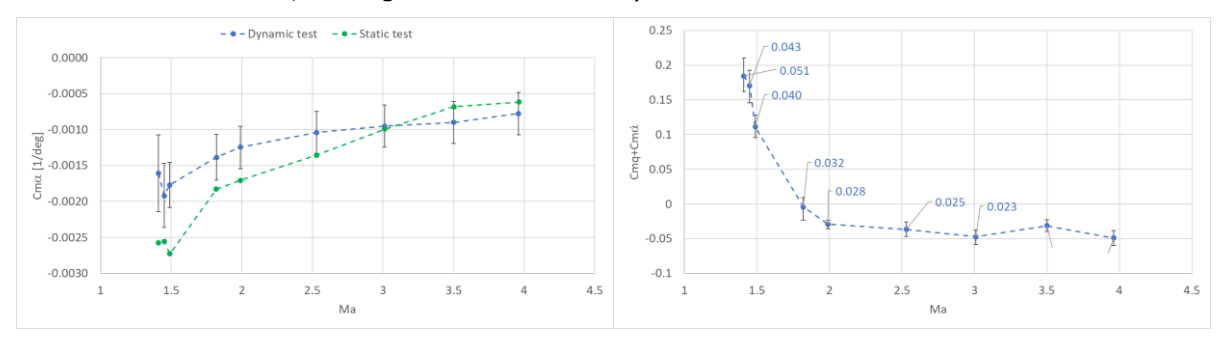


Fig. 18. Non-deformed aeroshape (left) and model mounted on the test device in TMK (right)

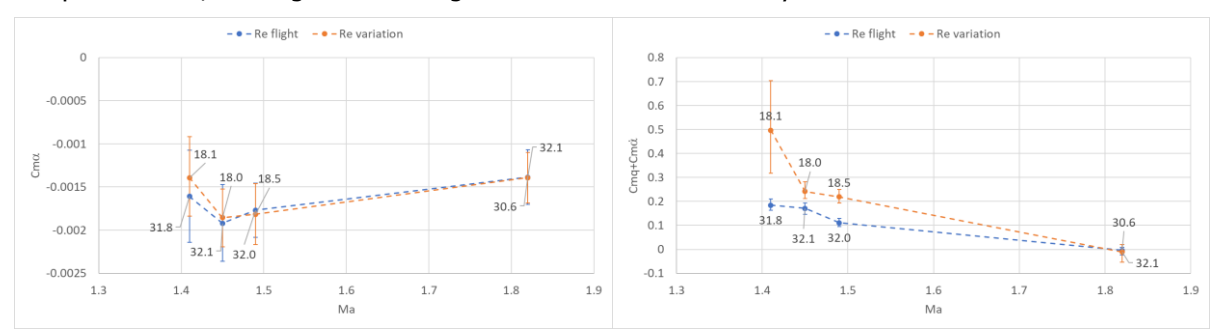
HiSST-2025-0092 Page | 11 Dynamic stability testing in DLR Wind Tunnels using a new free oscillation device Copyright © 2025 by author(s) The tests were conducted at Mach numbers from 1.4 to 4.0, first reproducing the flight Reynolds number conditions. The aerodynamic stiffness coefficients obtained with CS1 are shown in Fig. 19 (left) as a function of Mach number and compared with the static test results. The dynamic and static data show close agreement, despite the different measurement techniques.

Fig. 19 (right) shows the aerodynamic damping coefficients as a function of Mach number, obtained with CS1, with the RFPs indicated. The results show that the capsule is dynamically stable between Mach 3.96 and 1.99, becomes dynamically neutral at Mach 1.82, and transitions to dynamically unstable at lower Mach numbers, although it remains statically stable.



**Fig. 19.** Aerodynamic stiffness coefficients (RFP indicated) (left) and Aerodynamic damping coefficients at flight Reynolds numbers (right)

In this test campaign, Reynolds number variation was performed by decreasing the tunnel pressure to investigate the influence on stability. The results in Fig. 20 reveal that the aerodynamic stiffness coefficients remain essentially unaffected by the Reynolds number variation (Fig. 20, left). In contrast, a clear trend is observed for the damping coefficients: at lower Reynolds numbers, the aerodynamic damping derivative increases in the low Mach number range (Fig. 20, right), indicating a stronger tendency toward dynamic instability. At higher Mach numbers, the Reynolds number effect appears less pronounced, although the investigated variation was relatively small.



**Fig. 20.** Influence of Reynolds numbers on aerodynamic stiffness coefficients (left) and on aerodynamic damping coefficients (Re indicated) (right)

# 5. Conclusion

A versatile test device based on the free oscillation technique with interchangeable cross-springs was developed to meet the need for dynamic stability investigations in wind tunnels. Its functionality was verified through tests with both winged and capsule-type configurations. The device significantly reduces planning and preparation time, thereby lowering overall test costs. If designed properly, the same wind tunnel models can be used for determination of static and dynamic stability. To further extend its applicability, a larger version of the dynamic test mechanism is planned for application with bigger models and higher aerodynamic loads.

Using this device, the aerodynamic dynamic stability of the ReFEx vehicle was experimentally investigated in TMK at Mach numbers from 1.4 to 2.5. Both aerodynamic stiffness and damping were found to be negative along the designed trajectory, demonstrating that the vehicle is statically and dynamically stable. Future work will focus on determining the roll stability characteristics, as the vehicle will perform a roll maneuver during flight.

A capsule-type model of the non-deformed IHS aeroshape, developed within the EFESTO-2 project, was tested in TMK at Mach numbers from 1.4 to 4.0. The aerodynamic stiffness was found to be negative across the entire Mach range. The damping coefficients were negative above Mach 1.82, became zero at Mach 1.82, and turned positive at lower Mach numbers. These characteristics must be considered in the design of the guidance, navigation, and control (GNC) system.

#### References

- [1] A. Gülhan, J. Klevanski and S. Willems, "Experimental Study of the Dynamic Stability of the EXOMARS Capsule," in 7th European Symposium on Aerothermodynamics, Brugge, Belgium, 9-12 May 2011.
- [2] A. Guelhan, J. Klevanski, T. Gawehn and M. Achner, "Damping Derivatives Tests on the IXV Re-Entry Vehicle in the DLR Trisonic Windtunnel TMK," DLR-DERIVAS-TN-003, 2014.
- [3] A. Gülhan, J. Klevanski and T. Gawehn, "Experimental Study on the Dynamic Stability of the IXV Configuration," in 8th European Symposium on Aerothermodynamics for Space Vehicles, Lissabon, Portugal, 2-6 March 2015.
- [4] T. Gawehn, "Experimental Study on Static and Dynamic Stability of a Blunt Body Configuration," in International Conference on Flight Vehicles, Aerothermodynamics and Re-entry Missions & Engineering, Monopoli, Italy, 2019.
- [5] T. Gawehn, D. Neeb, F. Tarfeld, A. Gülhan and etc, "Experimental investigation of the influence of the flow structure on the aerodynamic coefficients of the IXV vehicle," Shock Waves, no. DOI 10.1007/s00193-011-0326-y, pp. 253-266, 2011.
- [6] T. Gawehn, J. Zhai and M. Miketta, "Wind Tunnel Test Device for Determining Dynamic Invalties at a Wind Tunnel Model". EU Patent EP4592661 A1, 30 07 2025.
- [7] T. Gawehn, J. Zhai, P. Gruhn and A. Gülhan, "Aerodynamic wind tunnel testing of a generic Hypersonic Glide Vehicle," in the 4th International Conference on High-Speed Vehicle Science Technology, Tours, France, 22-26 September 2025.
- [8] P. Rickmers, W. Bauer, M. Sippel and S. Stappert, "Refex: Reusability flight experiment a flight experiment to demonstrate controlled aerodynamic flight from hypersonic to subsonic velocities with a winged rlv," in the 7th European Conference for Aeronautics and Space Sciences, Milan, Italien, 2017.
- [9] A. Flock, T. Thiele, D. Neeb and A. Gülhan, "Planned Wind Tunnel Experiments at DLR Köln for the Reusability Flight Experiment (ReFEx)," in International Conference on Flight Vehicles, Aerothermodynamics and Re-entry Missions & Engineering, Monopoli, Italien, 30 September 2019.
- [10] H. Esch, "Die 0.6-m x 0.6-m-Trisonische Meßstrecke (TMK) der DFVLR in Köln-Porz (Stand 1986)," DLR, 1986.
- [11] G. Guidotti, "The EFESTO project: Advanced European re-entry system based on inflatable heat shield," in 2nd International Conference on Flight Vehicles, Aerothermodynamics and Re-entry Missions & Engineering, Heilbronn, Germany, 2022.
- [12] Y. Prevereaud, Y. Dauvois, J. Zhai, T. Gawehn, G. Guidotti and G. Governale, "Numerical aeroshape characterization of an Inflatable Heat Shield reentry vehicle in the EFESTO-2 project," in 3rd International Conference on High-Speed Vehicle Science, Busan, Korea, 2024.
- [13] J. Zhai, T. Gawehn, A. Gülhan and Y. Prevereaud, "Experimental aeroshape characterization of an Inflatable Heat Shield re-entry vehicle in the EFESTO-2 project," in 3rd International Conference on High-Speed Vehicle Science Technology, Busan, Korea, 14-19 April 2024.

HiSST-2025-0092 Page | 13 Copyright © 2025 by author(s)